Nanoscale Schottky barrier mapping of thermally evaporated and sputter deposited W/Si(001) diodes using ballistic electron emission microscopy

Westly Nolting, Chris Durcan, and Avyaya J. Narasimham
College of Nanoscale Science and Engineering, University at Albany, SUNY, Albany, New York 12203

Vincent P. LaBella[a]
Colleges of Nanoscale Science and Engineering, SUNY Polytechnic Institute, Albany, New York 12203

Ballistic electron emission microscopy has been utilized to demonstrate differences in the interface electrostatics of tungsten-Si(001) Schottky diodes fabricated using two different deposition techniques: thermal evaporation using electron-beam heating and magnetron sputtering. A difference of 70 meV in the Schottky barrier heights is measured between the two techniques for both *p*- and *n*-type silicon even though the sum of *n*- and *p*-type Schottky barrier heights agrees with the band gap of silicon. Spatially resolved nanoscale maps of the Schottky barrier heights are uniform for the sputter film and are highly disordered for the e-beam film. Histograms of the barrier heights show a symmetric Gaussian like profile for the sputter film and a skewed lognormal distribution for e-beam film. A Monte-Carlo model is developed to simulate these histograms which give strong indication that localized elastic scattering is causing this skewing as forces the hot electrons to need a greater total energy to surmount the barrier. These differences are attributed to silicide formation from the unintentional substrate heating during the e-beam deposition, which is confirmed with transmission electron microscopy. © *2016 American Vacuum Society.*
[http://dx.doi.org/10.1116/1.4958721]

I. INTRODUCTION

The metal/semiconductor interface is a widely utilized rectifying junction found in numerous semiconductor devices, and improving our fundamental and practical knowledge is especially important as devices scale to the nanoscale. The Schottky barrier height of the metal/semiconductor system is determined by the metal's work function, the electron affinity of the semiconductor, and bonding or defects present at the interface.[1–4] Tungsten as the metal in Schottky diode has recently generated interest in semiconductor devices utilized in high power applications because of their capability to block high voltages at elevated temperatures and as raised source/drain contacts in sub-20 nm CMOS transistors.[5–7] Common techniques for metallization of high melting point metals such as tungsten are magnetron sputter and thermal evaporation using electron beam heating of the source material. Electron beam deposition is known to cause damage to the surface of the substrate from stray electron radiation.[8] In addition, it may cause unintentional heating of the substrate when the substrate to source distance is small, which is further exacerbated when depositing refractory metals which require a high temperature. Magnetron sputter is less thermally intensive for the substrate during deposition and when coupled with small deposition times should result in a more uniform interface.

Only a few studies exist of the electrostatics of the tungsten–silicon Schottky diodes using current–voltage or capacitance–voltage techniques.[9,10] These techniques are macroscopic techniques that provide an average measurement of the interface but do not provide information about the nanoscale fluctuations of the barrier height that may arise due to fluctuations in the composition, unintentional foreign species, or other defects due to differences in processing.[11–14] This insight would be insightful as contact areas are continuously scaled to the nanometer length scale. Schottky barrier mapping with Ballistic electron emission microscopy (BEEM) is a proven technique that provides nanoscale resolution of the electrostatics of an interface.[15–20] BEEM is a scanning tunneling microscopy (STM) based technique which injects electrons into the metal layer of a metal–semiconductor interface and collects the electrons that overcomes the barrier height.[21] In BEEM, the STM tip is positioned along the surface while a voltage is applied between the tip and the grounded metal surface generating a tunneling current shown in Fig. 1. If the energy of the electron is high enough, the electron will have sufficient perpendicular momentum to pass from the metal to the semiconductor and be collected as BEEM current (I_B). Previous Schottky barrier mapping of e-beam deposited W/Si interfaces have been performed which show a highly disorder interface and a skewed distribution of barrier heights with little attribution to its underlying cause other than compositional fluctuations or defects altering the electrostatics of the interface.[17,18]

In this article, stark differences in the interface electrostatics are observed with nanoscale resolution using BEEM on tungsten silicon Schottky contacts. The sputter deposited tungsten films show a structurally abrupt interface and spatially uniform Schottky barriers, whereas the e-beam deposited tungsten shows an intermixed interface and a spatially inhomogeneous Schottky barriers. The nonuniformity of the e-beam sample is attributed to unintentional substrate heating during deposition due to the proximity of the substrate and source that promotes silicide formation. The electrostatic

a)Electronic mail: vlabella@sunypoly.edu
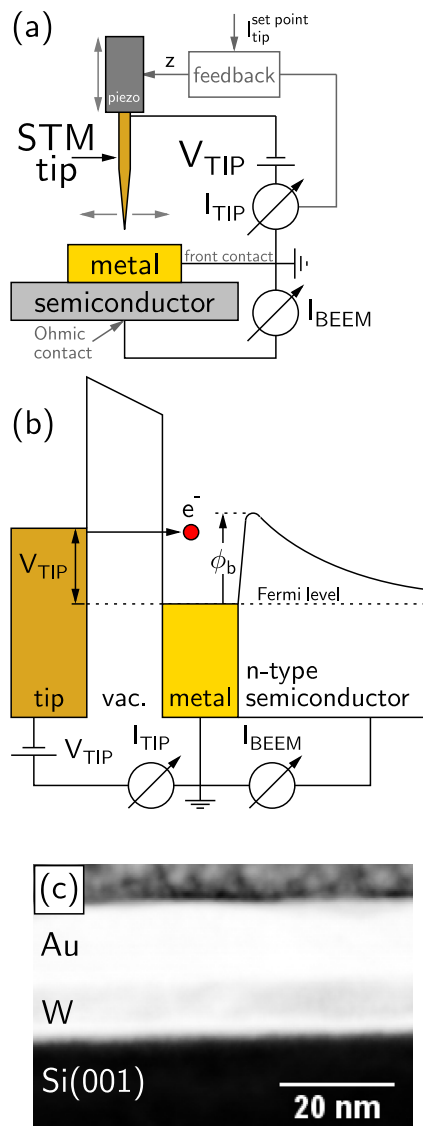
(a)

(b)

(c)

Au

W

Si(001)

20 nm

FIG. 1. (Color online) (a) Wiring schematic of the BEEM experimental set-up. The STM tip is utilized to tunnel inject hot electrons into a metal–semi-conductor structure. (b) Energy band diagram of the BEEM experiment. (c) TEM image of sputter tungsten sample.

nonuniformity of the e-beam sample is attributed to this intermixing as well as elastic scattering of the hot electrons in the disordered film, which is corroborated with a Monte-Carlo model. Interestingly, the sum of the *n* and *p*-type Schottky barriers is in good agreement with the band gap of silicon for both samples.

II. EXPERIMENT

The tungsten/silicon Schottky diodes were fabricated with two different deposition techniques in separate chambers; thermal evaporation using electron beam deposition heating of the source material (e-beam), and radio frequency magnetron sputtering (sputter). The e-beam deposition was performed under 10^{-7} mbar with a substrate to source distance of 0.5 m. The sputter deposition was performed in an

ultrahigh vacuum (UHV) system with a base pressure in the 10^{-9} mbar range. The same high resistive (10–100 Ω cm) *p*- and *n*-type Si(001) substrates were utilized for both depositions resulting in four separate samples. Prior to deposition, the silicon surface was cleaned with a standard HF acid treatment to remove any native oxide. The substrate was covered with a shadow mask to create 1 mm × 2 mm diodes. The e-beam sample consisted of 5 nm of tungsten with a 10 nm Au capping layer, and the sputter deposited sample consisted of 6 nm of tungsten with a 8 nm Au capping layer. The capping layer prevented the oxidation of the W layer. The thickness of the metal layers was confirmed with Rutherford backscattering spectrometry and energy-dispersive X-ray TEM in a JOEL Titan.

A modified low temperature UHV STM (Omicron) was used for all BEEM and ballistic hole emission microscopy (BHEM) measurements with a base pressure in the 10^{-11} mbar range.[22] The sample was mounted on a specially designed BEEM plate to ensure proper grounding, allowing independent measurement of both tunneling current, I_{tip} and BEEM current, I_B. An ohmic contact to the semiconductor was made by cold-pressing indium between the plate and the backside of the silicon. Two-point IV measurements were acquired at room temperature to ensure rectification. The sample was then loaded into the UHV chamber and onto the STM stage within 3 h of deposition and immediately cooled down to 78 K, and then, BEEM and BHEM measurements were performed. Individual BEEM spectra were acquired at unique tip locations every 11.7 nm on a grid over a 1 μm × 1 μm area by sweeping the voltage from 0.2 to 2 V for the *n*-type diodes, and −0.2 to −2 V for the *p*-type diodes. This resulted in 7225 spectra being collected over a 24 h period. Constant tunneling currents of 30 and 5 nA were utilized for the e-beam and sputter deposited samples, respectively. All measurements were taken in the absence of ambient light.

The individual spectra were then averaged into one spectra for each sample, and then, all the spectra were fit to a simplified BEEM model $I_B = A(V_t - \phi_b)^n$, where V_t is the tip bias, *n* is a model exponent, *A* is the amplitude, and ϕ_b is the Schottky barrier height. Fits were performed by linearizing the BEEM spectra and using a standard linear regression, which returns, ϕ_b, *A*, and a corresponding R^2 value, indicating the quality of fit. Best fits were selected over 0.2 eV window with a maximum R^2 value, where R^2 value less than 0.6 were considered unable to be fit.

III. RESULTS

The cross sectional TEM image of the sputter sample shows distinct regions of metal with abrupt interfaces between the Au, W, and Si and is displayed in Fig. 1(c), and TEM images of the e-beam deposited samples display an intermixed region of W and Si and have been previously published.[17,18] The averaged BEEM spectra and corresponding fits indicating the Schottky barrier height for all four samples are plotted linearized and displayed in Fig. 2. Each spectra is an average of 7225 spectra and fit to *n* = 5/2, with

an R^2 value of 0.999 or greater. The barrier heights for both the p and n-type sputter samples are both about 0.07 eV less than the e-beam deposited samples. The solid line indicates the region of fit (0.2 eV), and the dotted line indicates the extrapolation of the fit to the x-axis intercept or ϕ_b. The extrapolation region is smallest (0.02 eV) for the n-type sputter sample and larger for the other samples (0.05–0.07 eV). All four average spectra are plotted together in Fig. 3 to demonstrate the shift in the barrier heights and similarities in the sum of the barriers. Fits using $n = 2$ were also performed and resulted in a sum of barrier heights that was 0.07 eV higher than the band gap of silicon and not considered any further.

The spatial map of the Schottky barrier height obtained from the fitting of each individual spectra for all four samples is displayed in Fig. 4. The maps of the sputter deposited samples show a very homogeneous distribution of Schottky barrier heights, whereas the maps of the e-beam deposited sample show a spatially inhomogeneous distribution with several localized regions with barrier heights higher than that obtained from fits to the average.

The histograms of all the barrier heights for all four samples along with the mean barrier height and standard deviation of the distribution are plotted in Fig. 5. The histograms for the sputter deposited samples show a symmetric distribution with a mean barrier height very close to the barrier height obtained from the fit to the averaged spectra. The distribution of the n-type sputter sample is the narrowest and this increases for the p-type distribution. The distributions for the e-beam samples show a much broader distribution when compared to the sputter samples and are asymmetric with a long tail to higher (lower) energies for the n-type (p-type) samples. The sputter samples' mean barrier height is higher (lower) than the Schottky barrier height obtained from the fit to the averaged spectra for the n-type (p-type) samples. All samples are fit to a lognormal probability distribution function

$$PDF\left(V_{tip}, a, b, \bar{\phi}_b\right) = \frac{b\, e^{-\frac{1}{2}\left(a + b\log\left(V_{tip} - \bar{\phi}_b\right)\right)^2}}{\sqrt{2\pi}\left(V_{tip} - \bar{\phi}_b\right)}, \qquad (1)$$
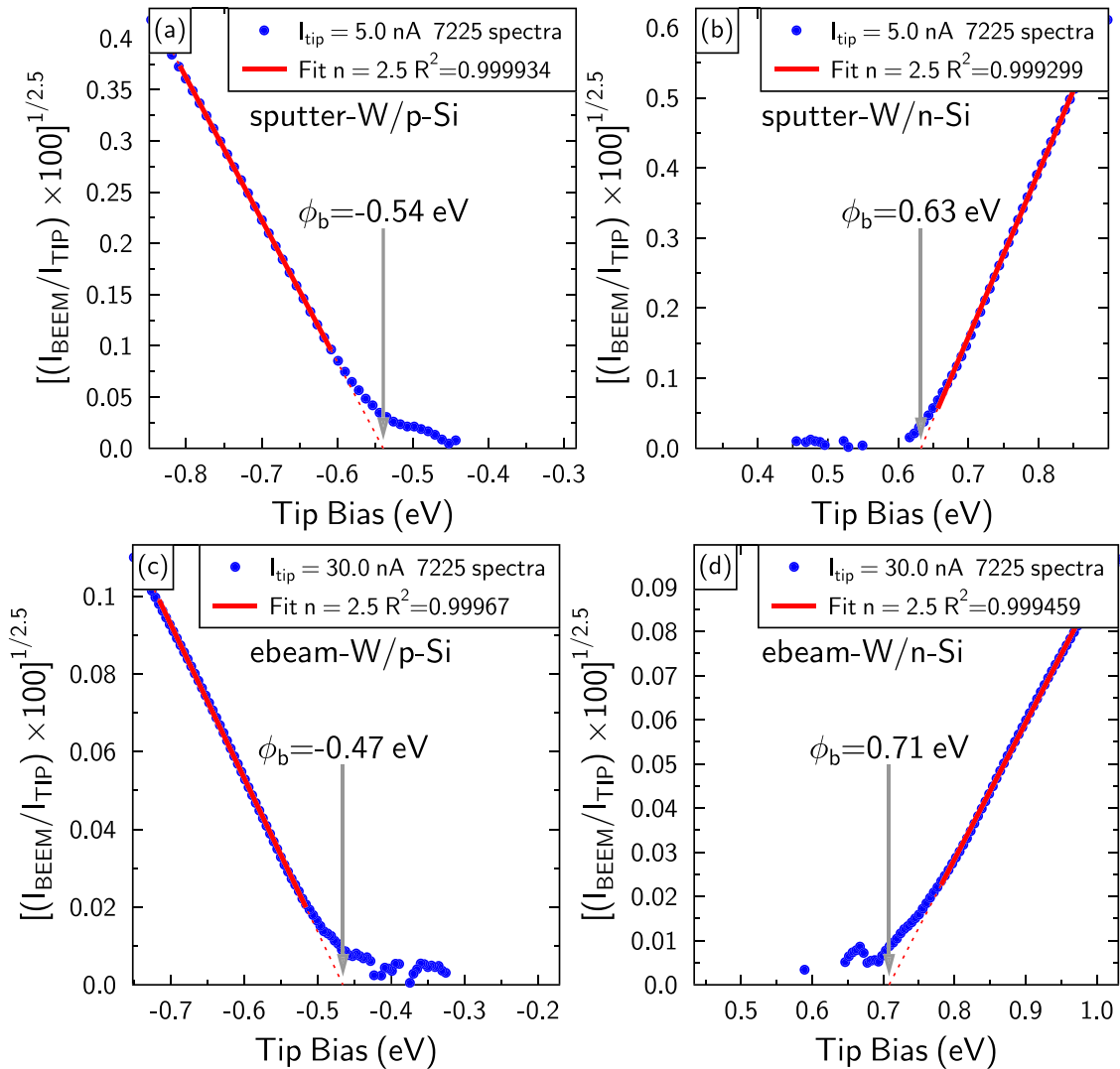

FIG. 2. (Color online) (a) Linearized fit of BHEM spectra of p-type sputter Schottky diode using exponent of n = 2.5. (b) n-type linearized fit of sputter Schottky BEEM spectra. (c) p-type e-beam linearized fit of BHEM spectra showing an increased Schottky barrier height compared to its sputter equivalent. (d) n-type e-beam linearized fit of BEEM spectra.
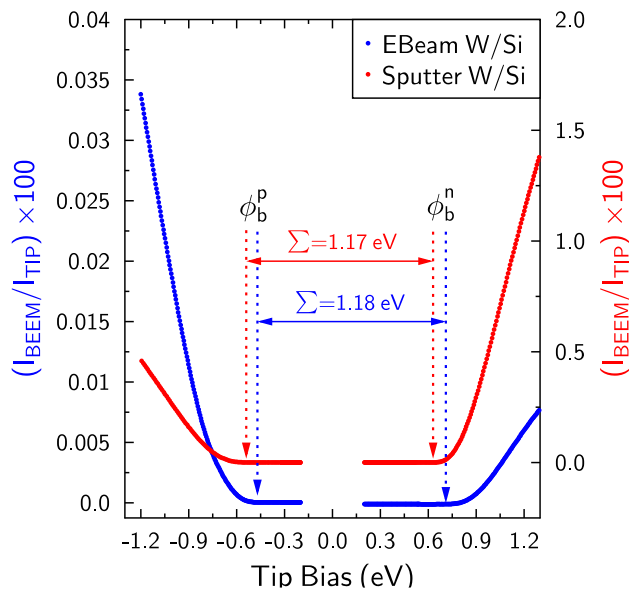
FIG. 3. (Color online) Average spectra of all four samples on the same plot to demonstrate shift in barrier heights and agreement to the band gap of silicon. Each curve is plotted vs percent transmission of the BEEM current.

where a is the shape parameter, b is the scale parameter, $\bar{\phi}_b$ is the average measured barrier height.[23] A Monte-Carlo model was developed to simulate the histogram based on adjustable elastic Γ_e and inelastic scattering rates Γ_i as well as a Gaussian distribution σ_{ϕ_b} of barrier heights at the interface. Its results are plotted along with the identical lognormal PDF from the e-beam histograms and are displayed in Fig. 6.

The Schottky barrier heights are plotted versus R^2 value for all the individual fits along with lines indicating the mean R^2 and mean Schottky barrier height and displayed in Fig. 7. The sputter deposited samples show a tight locus of points around the intersection of the average values, whereas the e-beam samples show much more diffuse distribution of points. All the plots show distributions of values about the locus with little trend of correlation between the two, but the e-beam samples do show much lower R^2 values.

IV. DISCUSSION

Previous IV studies of sputter deposited W/Si(001) Schottky diodes measure barrier heights of 0.65 eV and −0.5 eV for n-Si and p-Si, respectively.[9,10] These barrier heights are in good agreement with the sputter deposited tungsten samples reported here. Interestingly, the e-beam samples show a 70 meV shift to higher energies, which was also observed with sputter and then annealed tungsten.[10] In addition, 60× less transmission is observed in the e-beam samples (1% for sputter to 0.017% for e-beam at 1 V). The most likely cause of this barrier shift and decrease in current for the e-beam samples is silicide formation from unintentional heating during electron beam deposition.[8] Tungsten is a high Z refractory metal which requires a high emission current output from the electron beam to heat the tungsten source to a high enough temperature for deposition onto the substrate. This would

cause unintentional radiative heating of the substrate due to its proximity to the source which would promote intermixing and the formation of a silicide. The TEM images support this finding as they show a more intermixed interface for the e-beam sample[17] when compared to sputter sample, which shows a very abrupt interface as seen in Fig. 1. This silicide formation has a dramatic effect on the barrier heights measured by BEEM which is independent of carrier type as the sum of the p and n barrier heights for all samples is in good agreement with the band gap of silicon.

The average spectra and all individual spectra were fit to an $n = 5/2$ exponent to the simplified BEEM power-law model. In general, there are two values utilized in the BEEM model, $n = 2$ Bell–Kaiser (BK) and $n = 5/2$ Prietsch–Ludeke (PL).[21,24] Both models assume no scattering within the metal, and the PL model adds energy dependent transmission coefficient for tunneling transport across the Schottky barrier. The PL model systematically lowers the Schottky barrier when compared to the BK model and provides better agreement with the silicon band gap at 78 K (1.166 eV for Si at 78 K) for both sets of samples as indicated in Fig. 3.[25] These samples are formed on low doped silicon that would result in a long depletion width which should inhibit tunneling. However, the thin interface silicide that forms is most likely affecting the characteristic of the threshold region in these BEEM spectra. Image force lowering of the barrier height for these low doped silicon substrates is calculated to lower the sum of both gaps by 0.013 eV.[15,26] This lowering does not alter the agreement with the gap significantly or alter the choice of BEEM model which is in contrast to Au, Ag, and Cu Schottky diodes on the same substrates where the BK model gave the best agreement with the Si band gap.[15]

The Schottky maps are a dramatic visual indication of the electrostatic character of the interface and how it depends upon its structure in Fig. 4. The maps for the sputter samples are uniform and homogeneous with minimal localized defects, whereas the e-beam sample shows a dramatic variation in the map with large portions at different heights and a high degree of localization. These variations in the barrier height are consistent with the larger degree of interface disorder present in the e-beam sample and can be caused by impurities, structural disorder from incomplete silicide formation, or any other defects that would alter the charge density near the interface.[27,28] In addition, elastic scattering of the hot electrons can cause higher thresholds in the BEEM spectra as it forces the electrons to need a greater total energy for transmission and can be supported by looking at the histograms of the barrier heights.

The symmetry, distribution width, and mean of the histogram of barrier heights contains a tremendous amount of information about the electrostatic character of the interface as a whole as seen in Fig. 5. The most symmetric histogram is for n-type sputter sample. It has the smallest σ and the mean of the distribution is equal to the fit to the average ($\bar{\phi}_b = \phi_b$). The corresponding fit to the average has the smallest extrapolation region, which arises from the narrow distribution as seen in Fig. 2(b). The p-type sputter sample also exhibits similar features but with a slightly larger σ and
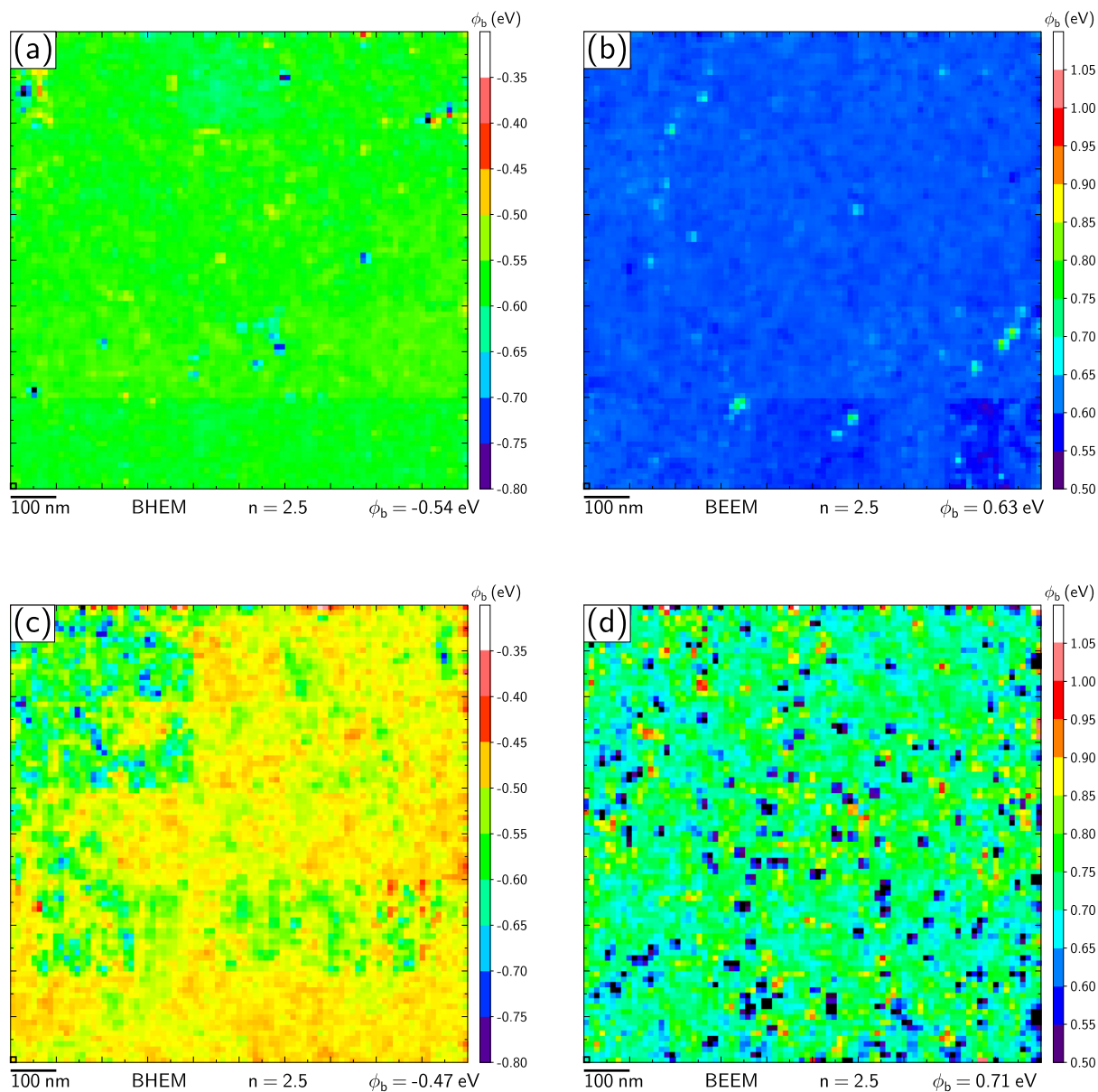
FIG. 4. (Color online) Each map displayed is representative of the electrostatic interface. (a) and (b) BHEM and BEEM measurements show a uniform interface for sputter. (c) and (d) e-beam samples show a very disordered interface caused by a change in the interface chemistry during deposition.

very small (0.01 eV) difference between $\bar{\phi}_b$ and ϕ_b. The extrapolation region of the fit to the average is also larger for the *p*-type sputter sample as seen in Fig. 2(a). The e-beam samples are dramatically different with much greater σ, a systematically lower mean Schottky that that obtained from a fit to the averaged spectra and highly asymmetric distributions. Both the extrapolation regions of the fits to the average spectra are large and similar to the *p*-type sputter sample as seen in Figs. 2(c) and 2(d). The extrapolation region arises from the width of the leading edge of the distributions, which is similar for these three samples. The averaging of multiple spectra with different onsets causes the average spectra to deviate from the linearity near the threshold and results in a fit to a Schottky barrier that is lower than the mean of the distribution, which is calculated from the fits to individual spectra.

A symmetric Gaussian like distribution is expected in barrier heights for metal semiconductor systems arising from variations in the interface structure where models based on interface dipoles have predicted this behavior and observed with BEEM.[3,20] This is partially the cause of the wider distributions of the e-beam samples as the incompletely formed silicide would have larger variations in stoichiometry and structure at the interface resulting in a broadening of the distribution of barrier heights. However, this effect cannot account for the long tail and asymmetry and tail in the distributions for the e-beam samples. The asymmetry in the distribution is attributed to elastic scattering that reduces the perpendicular momentum of the hot electrons, causing them to need a higher total energy to overcome the barrier. In contrast, few scattering events exist that would cause the electrons to need a *lower* total energy. This results in a skewed
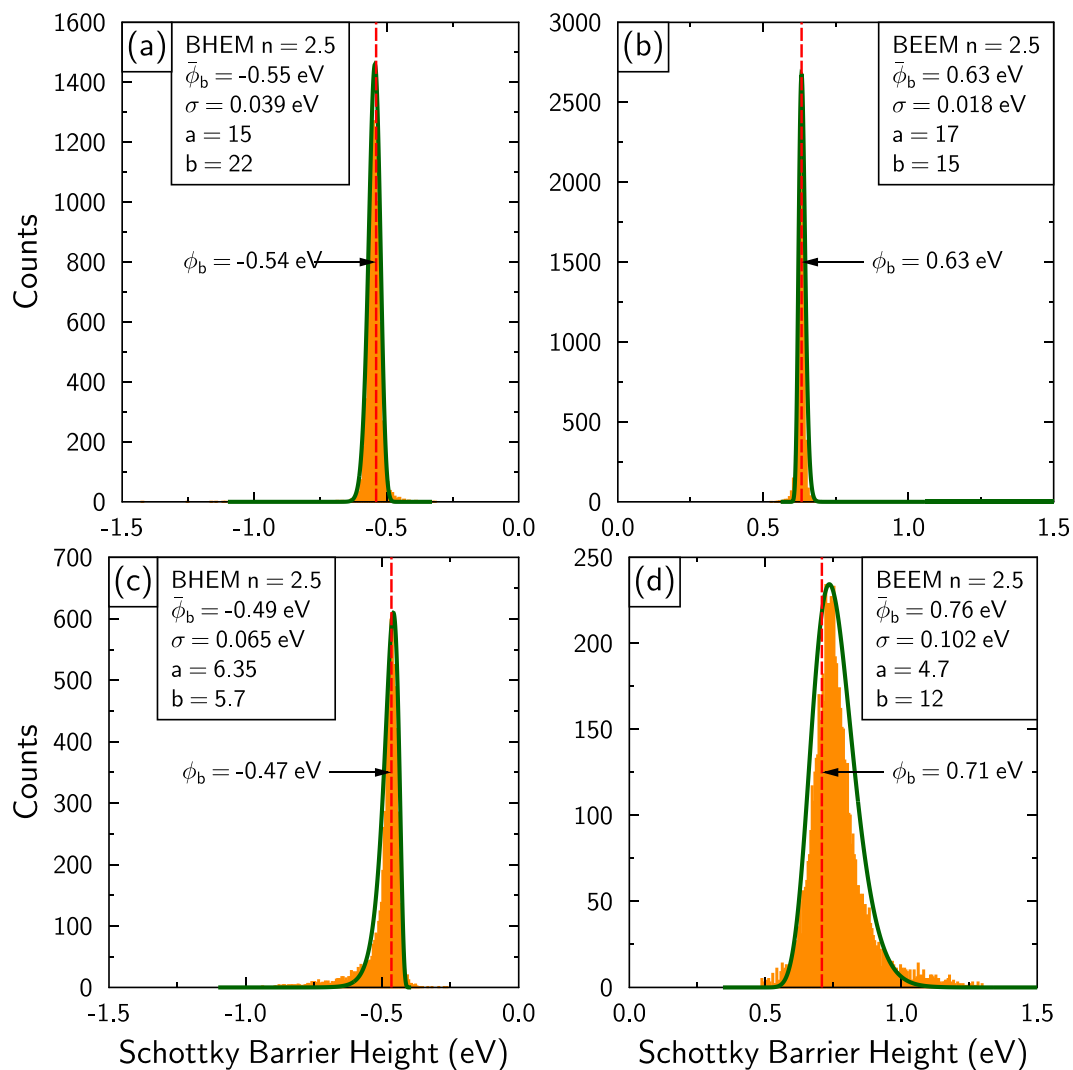
FIG. 5. (Color online) Histogram of the Schottky barrier heights from fits to the individual spectra. (a) and (b) are for the sputter sample and show a symmetric and narrow Gaussian-like distribution and good agreement between the mean Schottky and fit to the average. (c) and (d) are for the e-beam sample show a skewed asymmetric distribution attributed to elastic scattering of the hot electrons. The lines plotted are fits to a lognormal probability distribution function.

lognormal like asymmetrical distribution. Each histogram is fit with the lognormal probability density function in Eq. (1) and is indicated by the curves in Fig. 5.

To further enhance this argument, a Monte-Carlo model was developed which produces a histogram of barrier heights to compare to the measured values. This model assumes a Gaussian distribution of barrier heights with an adjustable standard deviation σ and adjustable elastic Γ_e and inelastic Γ_i scattering rates. Millions of electrons are generated with energies ranging from 0.2 to 1.5 eV and then randomly scattered by changing its incident angle with the interface by a small random scattering angle for elastic scattering. Inelastic scattering is performed randomly by subtracting some finite energy as well as randomly assigning a scattering angle. The final momentum normal to the interface is utilized to determine if the electron is able to overcome the barrier and that energy is recorded in the histogram as the local barrier height. For n-type e-beam sample, $\Gamma_e = 45\%$ and $\Gamma_i = 20\%$ give the best fit to the PDF used to fit the BEEM data, and for the p-type sample, these values are $\Gamma_e = 31\%$ and

$\Gamma_i = 19\%$ as indicated in Fig. 6. Skewing is not observed if $\Gamma_e = 0$, giving indication that the observed skewing and high energy tail in the BEEM data arises from localized elastic scattering. The localized nature of BEEM and the recording and fitting of individual spectra from a uniformly spaced grid provides this insight which is obfuscated in the averaged spectra.

The plots of the R^2 values of the fits versus Schottky barriers further support the observation that the disorder in the e-beam sample is affecting the interface electrostatics as shown in Fig. 7. For the p-type e-beam sample, the width of the R^2 distribution is over two times greater than the sputter sample as well as five times greater for the n-type samples. However, in each sample, little correlation is seen between both parameters, indicating that high quality fits are obtained throughout the range of barrier heights observed.

V. CONCLUSION

Dramatic differences in the interface electrostatics of W/Si(001) Schottky diodes are observed with nanoscale
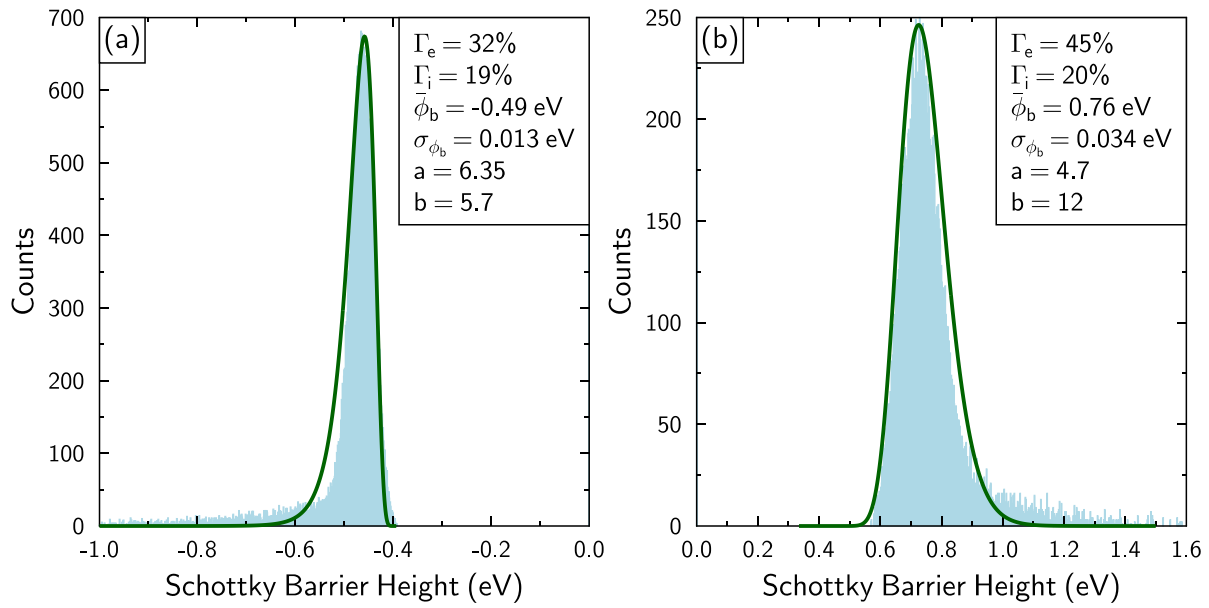
FIG. 6. (Color online) Results of the Monte-Carlo model and lognormal PDFs. (a) Simulated BEEM histogram for e-beam W/p-Si(001) with 32% elastic scattering and 19% inelastic scattering. (b) Simulated BEEM histogram for the e-beam W/*n*-Si(001) with 45% elastic scattering and 20% inelastic scattering.
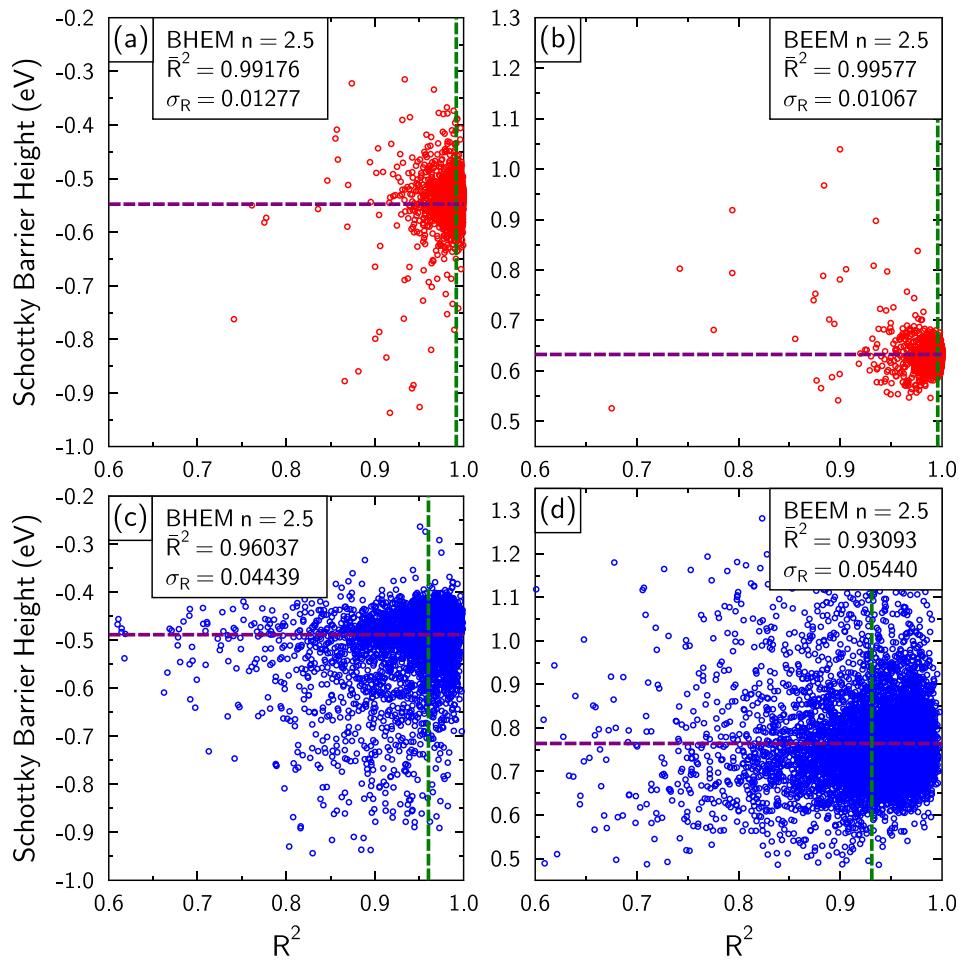

FIG. 7. (Color online) R^2 vs Schottky barrier height for all samples. In the case of sputter (a) and (b), the Schottky barrier heights fits are associated with a tight distribution around the average R^2 value. Both (c) and (d) e-beam samples exhibit a broad distribution of R^2 values which correspond to a wider range of Schottky barrier heights.

resolution using BEEM. The sputter deposited diodes show a structurally abrupt interface and spatially uniform Schottky barriers, whereas the e-beam deposited tungsten shows an intermixed interface and a spatially inhomogeneous Schottky barriers. The sum of the n and p-type Schottky barriers is in good agreement with the band gap of silicon for both samples, but the sputtered samples show a 70 meV shift to lower barrier heights. The structural nonuniformity of the e-beam sample is attributed to silicide formation from unintentional substrate heating during deposition. The electrostatic nonuniformity of the e-beam sample arises from this intermixing as well as an increase in elastic scattering of the hot electrons in the disordered film. Histograms of the barrier heights show a symmetric Gaussian like profile for the sputter film and a lognormal distribution for e-beam film, arising from elastic and inelastic scattering of the hot electrons indicated by the Monte-Carlo model. These results demonstrate the sensitivity and insight that fitting thousands of individual BEEM spectra over a regularly spaced grid can provide for the technologically important Schottky diode.

ACKNOWLEDGMENTS

[1] J. Tersoff, Phys. Rev. Lett. **52**, 465 (1984).
[2] J. Tersoff, Phys. Rev. B **32**, 6968 (1985).
[3] R. T. Tung, Mater. Sci. Eng. **35**, 1 (2001).
[4] R. T. Tung, Phys. Rev. B **45**, 13509 (1992).
[5] A. F. Hamida, Z. Ouennoughi, A. Sellai, R. Weiss, and H. Ryssel, Semicond. Sci. Technol. **23**, 045005 (2008).
[6] R. Weiss, L. Freyb, and H. Ryssel, Appl. Surf. Sci. **184**, 413 (2001).
[7] M. Takahashi, T. Ohno, Y. Sakakibara, and K. Takayama, IEEE Trans. Electron Devices **48**, 1380 (2001).
[8] M. Mamor, F. D. Auret, S. A. Goodman, and G. Myburg, Appl. Phys. Lett. **72**, 1069 (1998).
[9] M. Khaidar, A. Essafti, A. Bennouna, E. L. Ameziane, and M. Brunel, J. Appl. Phys. **65**, 3248 (1989).
[10] M. Aboelfotoh, J. Appl. Phys. **66**, 262 (1989).
[11] R. T. Tung, J. Vac. Sci. Technol., B **2**, 465 (1984).
[12] M. O. Aboelfotoh and B. G. Svensson, Semicond. Sci. Technol. **6**, 647 (1991).
[13] T. Arizumi and M. Hirose, Jpn. J. Appl. Phys., Part 1 **8**, 749 (1969).
[14] S. M. M. Coelho, F. D. Auret, P. J. J. van Rensberg, C. Nyamhere, J. M. Nel, and M. Hayes, Phys. Status Solidi C **5**, 626 (2008).
[15] R. Balsano, A. Matsubayashi, and V. P. LaBella, AIP Adv. **3**, 112110 (2013).
[16] R. Balsano, C. Durcan, A. Matsubayashi, A. J. Narasimham, and V. P. LaBella, J. Appl. Phys. **119**, 095302 (2016).
[17] C. A. Durcan, R. Balsano, and V. P. LaBella, J. Appl. Phys. **116**, 023705 (2014).
[18] C. A. Durcan, R. Balsano, and V. P. LaBella, J. Appl. Phys. **117**, 245306 (2015).
[19] C. Tivarus, J. P. Pelz, M. K. Hudait, and S. A. Ringel, Phys. Rev. Lett. **94**, 206803 (2005).
[20] H. J. Im, Y. Ding, J. P. Pelz, and W. J. Choyke, Phys. Rev. B **64**, 075310 (2001).
[21] L. D. Bell and W. J. Kaiser, Phys. Rev. Lett. **61**, 2368 (1988).
[22] M. Krause, A. Stollenwerk, C. Awo-Affouda, B. Maclean, and V. P. LaBella, J. Vac. Sci. Technol., B **23**, 1684 (2005).
[23] N. L. Johnson, S. Kotz, and N. Balakrishnan, *Continuous Univariate Distributions* (Wiley, New York, 1994).
[24] R. Ludeke and M. Prietsch, J. Vac. Sci. Technol., A **9**, 885 (1991).
[25] W. Bludau, A. Onton, and W. Heinke, J. Appl. Phys. **45**, 1846 (1974).
[26] S. M. Sze, *Physics of Semiconductor Devices* (Wiley, New York, 1981).
[27] F. D. Auret and P. M. Mooney, J. Appl. Phys. **55**, 988 (1984).
[28] F. D. Auret and P. M. Mooney, J. Appl. Phys. **55**, 984 (1984).